Accounting for the mechanical response of the cell membrane during the uptake of random nanoparticles

Sarah Iaquinta, Shahram Khazaie, Frédéric Jacquemin, Sylvain Fréour

OVERLAY

Journal of Theoretical, Computational and Applied Mechanics

JTCAM

DIAMOND OPEN ACCESS

Identifiers
DOI 10.46298/jtcam.12489
HAL hal-04266009v2

History
Received Oct 31, 2023
Accepted Feb 21, 2024
Published Sep 15, 2024

Associate Editor
Anna Pandolfi

Reviewers
Anonymous
Anonymous

Open Review
HAL hal-04576826

Supplementary Material
Software
SWHID [SoftwareHeritage]
Data
DOI 10.5281/zenodo.12519966

Accounting for the adaptation of cell membrane adhesion during the uptake of random nanoparticles

Sarah Iaquinta, Shahram Khazaie, Sylvain Fréour, and Frédéric Jacquemin

Nantes Université, Ecole Centrale Nantes, CNRS, GeM, UMR 6183, F-44600 Saint-Nazaire, France

Problem In order to improve the efficiency of the delivery of cancer treatments to cancer cells, the cellular uptake of nanoparticles (NPs), used as drug delivery systems, is numerically investigated through a mechanical approach. An overall challenge of cancer therapy is to optimize the NP's mechanical and geometrical properties, focusing on cell-NP adhesion, membrane tension and NP's aspect ratio, to enhance their entry into cancer cells while avoiding benign ones. In previous studies, the mechanical properties are modeled as constant during the process of cellular uptake. However, recent observations of the displacement of the membrane's constituents towards the region in the cell membrane where the uptake of the NPs takes place show that the adhesion between the NP and the membrane vary during this process.
Reason for writing The important contribution of adhesion to the wrapping process is already well documented in literature. It is therefore crucial to model this parameter properly as the conclusions made with a constant adhesion model may not be accurate compared to reality.
Methodology Based on the existing knowledge on the reaction of membrane constituents to interaction with NPs, a 3-parameter sigmoidal function, accounting for the delay, amplitude, and speed of the reaction, has been used to model the evolution of adhesion. A variance-based sensitivity analysis has then been performed in order to quantify the influence of these parameters on the outputs of the model.
Results It was found that the introduction of a variable adhesion tends to alter the predictions of endocytosis of NPs. The contribution of the amplitude and delay is respectively 0.32 and 0.43 times as important as that of the NP's aspect ratio, which is the prominent parameter. The influence of the slope of the transition is the least important parameter and does not appear to contribute to endocytosis.
Implications Hence, models of the cellular uptake of NPs should use a variable, instead of constant, adhesion in order a representative as possible of the behavior of the cell membrane. The predictions are different from those obtained using a model with constant adhesion.

Keywords: cellular uptake, adhesion, mechano-adaptation, sensitivity analysis, meta-modeling

1 Introduction

Cancer, being a major disease worldwide (18 million new cases in 2020 (Ferlay et al. 2021)), has made oncology an expanding research field. Part of this research focuses on developing treatments (Sudhakar 2009). This study focuses on non-local cancers, *i.e.* those which have spread from one organ to the rest of the organism, or which are located in tissues like blood. This kind of cancer must be treated with therapies like chemotherapy (Nygren 2001; E. Chu 2017), hormonotherapy (Hellerstedt et al. 2002; Murphy et al. 2012) or immunotherapy (Schuster et al. 2006). More recently, targeted therapies (Gerber 2008) have emerged. They consist in using vectors, *e.g.* nanoparticle (NPs), in which the anti-cancer agent is placed (Briolay et al. 2021). The vector is coated with specific constituents, called ligands, that aim at targeting cancer cells. Once the cell is reached, several steps remain: the NP needs to adhere to the membrane and to be fully wrapped by the latter to ensure the cellular internalization. The wrapping of the NP takes place via a mechanical process, involving the bending of the membrane around the NP, and the adhesion bentween the NP and the membrane. Previous results showed that the wrapping is favored by an important capability of the membrane to bend and to adhere to the NP, along with a small membrane tension (Iaquinta et al. 2022). Once the vector is fully

Abbreviations

CI	confidence interval
MC	Monte Carlo
NP	nanoparticle
PCE	polynomial chaos expansion
qMC	quasi Monte Carlo

Symbols

ΔE	variation of potential energy
γ	adhesion
κ	bending rigidity
$\overline{\Delta E}$	normalized variation of potential energy
$\overline{\Gamma}$	random normalized adhesion
$\overline{\gamma}$	normalized adhesion
Γ_A	random ratio between final and initial normalized adhesion
$\overline{\gamma}_A$	ratio between final and initial normalized adhesion
Γ_D	random delay of the transition of adhesion
$\overline{\gamma}_D$	delay of the transition of adhesion
Γ_S	random curvature parameter for the transition of adhesion
$\overline{\gamma}_S$	curvature parameter for the transition of adhesion
$\overline{\Sigma}$	random normalized tension
$\overline{\sigma}$	normalized tension
$\overline{r}$	aspect ratio of the NP
ϕ_i	angle between the tangent and horizontal in region i
ψ_j	proportion of wrapping phase j
σ	tension
a	relative radius of the NP
f	wrapping degree
f_{inf}	inflection point of $\overline{\gamma}(f)$
l_i	length of region i
N	number of samples
p	circumference of the NP
Q_2	predictability factor
S_i	Sobol first order index with respect to input parameter i
s_i	arclength in region i
ST_i	total Sobol index with respect to input parameter i

wrapped, the agent enters the cell, causing its death or making its reproduction impossible. Unfortunately, the ligands may sometimes bond to receptors that are located in the membrane of healthy cells. As such, it is necessary to improve the precision of the targeting technique, in order to protect healthy cells from these agents. Moreover, discrepancies in the mechanical properties of healthy and cancer cells have been observed experimentally. Cancer cells are for instance less stiff compared to their healthy counterparts (Lekka et al. 2012; Lin et al. 2015; Hall 2009; Suresh 2007). In addition, they also adhere less to the extra-cellular medium (Yang et al. 2013; Haley et al. 2008; Kuo et al. 2018; Kanyo et al. 2020). It could therefore be theoretically possible to control the uptake of NPs by cells of different types based on a mechanical differentiation. Hence, experimental studies have been conducted in order to observe the effect of the properties of NPs on their entry into cells of different types (Canton et al. 2012; Wiegand et al. 2020; Schmid et al. 2014). However, such studies have several limitations, such as the experimental facilities, that do not enable to assess the mechanical properties of the investigated cells with accuracy and reproducibility (Rigato 2015; Vasir et al. 2008; Y.-S. Chu et al. 2005; Evans et al. 1987; Lekka et al. 2012). To overcome such practical challenges and to guide experimental work, models for the cellular uptake of NPs, focusing of the crucial wrapping step, have also been developed (S. Zhang et al. 2015). The main approaches are commonly used accordingly to the scale at which the problem is investigated and the chosen discretization. For instance, molecular dynamics approaches involve the representation of molecules or groups of molecules with their chemical interactions, while models at the scale of the NP involve a homogenized modeling of the NP and the membrane (S. Zhang et al. 2015). In this paper, a model at the scale of the NP (in opposition to those at the scale of the constituents of the cell membrane), is used. This kind of approach enables to simplify the problem by modeling the membrane as a thin line when its thickness, usually below 10 nm (Zhao et al. 2014), is small compared to the NP. To ensure this hypothesis is true, only NPs whose radius is larger than 100 nm are considered. Models at the scale of the NP have mostly been developed by Yi, Shi, et al. (2011) and were already presented in our previous article in a stochastic framework (Iaquinta et al. 2022). For these models to provide the most reliable predictions of the internalization of a NP, the input parameters must be defined accurately. As such, in this article, we present a model that accounts for the mechanical reaction of the membrane, triggered by the interaction with the NP. Accounting for this phenomenon in such a model is thus a novelty, and the consequences of this enrichment of the model are quantified via a variance-based sensitivity analysis. The objective of this article is to demonstrate the importance of accounting for variations in adhesion during wrapping.

This paper is organized as follows: Section 2 introduces the numerical model and Section 3 presents the adaptation of the membrane and the way it has been incorporated into the model. The effect of this new feature is investigated in Section 4, where sensitivity analyses on the internalization of circular and elliptic NPs are conducted. In Section 6, conclusions are drawn on the influence of the mechano-adaptation of the membrane on the predictions of the model.

2 Existing model

In (Iaquinta et al. 2022), we presented our model to investigate the wrapping of a rigid elliptic NP, whose circumference p is set to 200π nm (the circumference of a circular NP whose radius is 100 nm), by the membrane of a cell whose diameter is about 10 µm. These objects are schematically represented in Figure 1(a). The hypothesis of a rigid NP is made to reduce the number of parameters and focus on those relative to the cell membrane. The difference in the scales of the NP and that of the cell enables us to represent the cell membrane as a single thin line, instead of modeling each constituent. With this hypothesis, the behavior of the cell membrane is described by its bending rigidity κ, the adhesion γ between the cell and the NP, along with the membrane tension σ. The system, formed by the NP and the membrane, is therefore investigated through the variation of its potential energy, defined by the Canham-Helfrich Halmitonian (Seifert and Lipowsky 1990; Seifert 1991; Deserno and Bickel 2003; Deserno 2004; Helfrich 1973), as a function of the bending energy ΔE_b of the membrane, the energy related to its stretching ΔE_σ, and that due to its adhesion with the NP, ΔE_γ. The variation of the potential energy of the system reads

$$\Delta E = \underbrace{\overbrace{\frac{\kappa}{2}\int_0^{l_2}\dot{\phi}_{2r}^2 \mathrm{d}s_{2r}}^{\Delta E_{b_{2r}}} + \overbrace{\frac{\kappa}{2}\int_0^{l_2}\dot{\phi}_{2l}^2 \mathrm{d}s_{2l}}^{\Delta E_{b_{2l}}} + \overbrace{\frac{\kappa}{2}\int_0^{l_3}\dot{\phi}_{3}^2 \mathrm{d}s_{3}}^{\Delta E_{b_3}}}_{\Delta E_b} \underbrace{- \gamma l_3}_{\Delta E_\gamma} + \underbrace{\sigma(2l_2 + l_3 - r_{2r}(l_2) + r_{2l}(l_2))}_{\Delta E_\sigma}, \quad (1)$$

where s_i is the arclength, defined between 0 and l_i, ϕ_i is the angle between the tangent and the horizontal, as illustrated in Figure 1(b). The indices $i \in \{2r, 2l, 3\}$ correspond to the different regions of the system. The regions $2r$ and $2l$ stand for the free membrane, located at the right and left sides of the NP, and 3 represents for the contact region between the NP and the membrane.

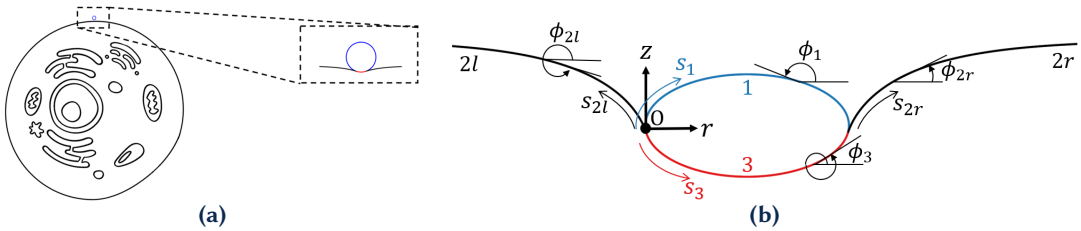

Figure 1 Considerations for the model. (a) Scale of the model. (b) System of coordinates used to describe the wrapping of the NP by the cell membrane.

Using the hypothesis of symmetry between the two sides of the membrane yields $l_{2r} = l_{2l} = l_2$ and $\phi_{2r} + \phi_{2l} = 2\pi$. As such, Equation (1) simplifies to

$$\Delta E = \underbrace{\overbrace{\kappa\int_0^{l_2}\dot{\phi}_{2r}^2 \mathrm{d}s_{2r}}^{\Delta E_{b_2}} + \overbrace{\frac{\kappa}{2}\int_0^{l_3}\dot{\phi}_{3}^2 \mathrm{d}s_{3}}^{\Delta E_{b_3}}}_{\Delta E_b} \underbrace{- \gamma l_3}_{\Delta E_\gamma} + \underbrace{\sigma(2l_2 + l_3 - r_{2r}(l_2) + r_{2l}(l_2))}_{\Delta E_\sigma}. \quad (2)$$

Following (Yi, Shi, et al. 2011), ΔE is adimensionalized in order to obtain an expression that is independent of the size of the NP. As such, $\overline{\Delta E}$ is introduced as $\overline{\Delta E} = 2a\Delta E\kappa^{-1}$, along with $\bar{\gamma} = 2a^2\gamma\kappa^{-1}$ and $\bar{\sigma} = 2a^2\sigma\kappa^{-1}$, where a is the relative radius of the NP, defined as the ratio between the circumference p of the NP and 2π. Finally, $\overline{\Delta E}$ reads

$$\overline{\Delta E} = \underbrace{\overbrace{\frac{a}{4}\int_0^{l_3}\dot{\phi}_{3}^2 \mathrm{d}s_{3}}^{\overline{\Delta E}_{b_3}} + \overbrace{\frac{a}{2}\int_0^{l_2}\dot{\phi}_{2r}^2 \mathrm{d}s_{2r}}^{\overline{\Delta E}_{b_2}}}_{\overline{\Delta E}_b} \underbrace{- \frac{1}{4a}\bar{\gamma} l_3}_{\overline{\Delta E}_{\bar{\gamma}}} + \underbrace{\frac{1}{4a}\bar{\sigma}(2l_2 + l_3 - r_{2r}(l_2) + r_{2l}(l_2))}_{\overline{\Delta E}_{\bar{\sigma}}}. \quad (3)$$

Using the expression of $\overline{\Delta E}$, the system is at a stable equilibrium as $\overline{\Delta E}$ reaches its first local minimum in terms of the wrapping degree f of the NP, defined as $f = l_3 p^{-1}$. An illustration of the minima and equilibrium position of the system, based on the evolution of $\overline{\Delta E}$ in terms of f, is provided in Figure 2(a). The wrapping degree at which the equilibrium is reached is henceforth denoted by $\tilde{f}$. Once $\tilde{f}$ is determined, the shape of the system is observed and the phase is therefore defined. If $\tilde{f} < 0.2$, the NP is in phase 1, *i.e.* no wrapping. The NP is in phase 3 (full wrapping) if the two sides of the free membrane have merged above the NP. The NP is in phase 2 (partial wrapping), otherwise. The definition of these phases is illustrated in Figure 2(b).

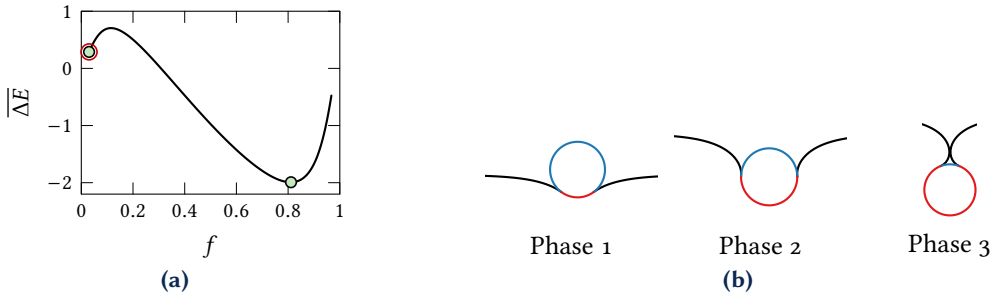

Figure 2 Definition of the equilibrium. (a) $\overline{\Delta E}$ in terms of the wrapping degree f, for $(\overline{\gamma}, \overline{\sigma}, \overline{r}) = (6, 2, 0.3)$. The single circles correspond to the minima of energy, while the double circle stands for the equilibrium (first local minimum). (b) Description of the wrapping phases.

3 Mechanical adaptation of the membrane

3.1 Description of the phenomenon

In this section, we present the observations, made from the literature, that led us to face the need for modeling the mechanical response of the membrane after contact with the NP.

3.1.1 Membrane tension

The cell contour is constituted of several irregularities, mostly invaginations, and protuberances, as illustrated in Figure 3(a). These are the so-called membrane reservoirs (Staykova et al. 2013; Kosmalska et al. 2015; Ferguson et al. 2017; Sinha et al. 2011; Rädler et al. 1995), that are unfolded (see Figure 3(b)) when the membrane is stretched to wrap the NP. As a consequence, the membrane tension does not increase during the wrapping of the NP, yielding $\overline{\sigma}(f) := \overline{\sigma}_0$, that will hereinafter be denoted as $\overline{\sigma}$.

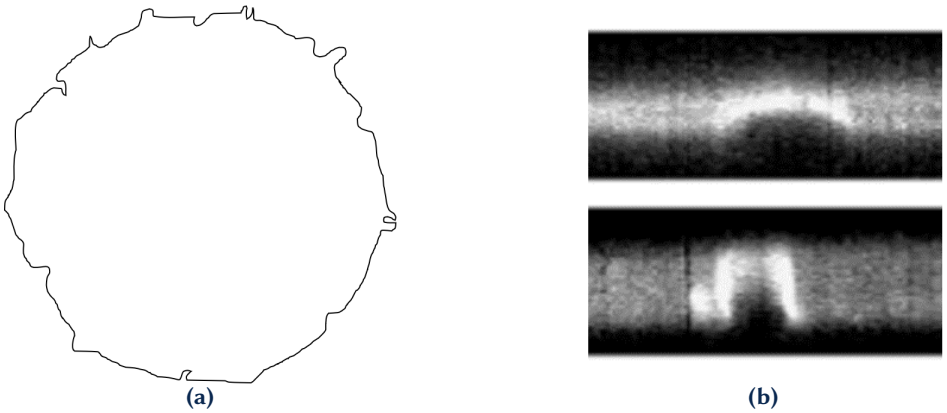

Figure 3 Cell membrane geometry. (a) Simplified illustration of the nonsmooth shape of a cell. (b) Observation of a reservoir on a stretched membrane, (top) during and (bottom) after unfolding, reproduced from (Kosmalska et al. 2015).

3.1.2 NP-membrane adhesion

NP-membrane adhesion has two main sources: the interactions between the membrane receptor and the ligands on the surface of NP, and interactions between other molecules from the NP and the membrane, such as van der Waals, electrostatic bonds or hydrophobic interactions (S. Zhang et al. 2015; R. Zhang et al. 2019). The movement of membrane receptors has been observed and studied in the case of the interaction with a NP (Yi and Gao 2017; Decuzzi et al. 2008) and also for the adhesion of a cell to a substrate (Yi and Gao 2017; Freund 2004; Serpelloni et al. 2021). A schematic illustration of this phenomenon is provided in Figure 4.

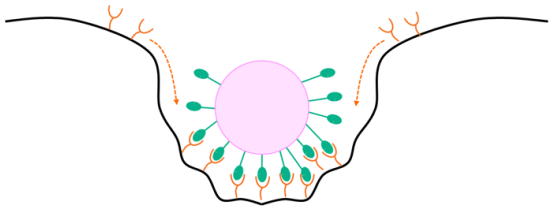

Figure 4 Displacement of the receptors to the contact region during the wrapping of the NP.

Furthermore, the constituents of the membrane are reorganized laterally. As such, proteins and lipids may reach the contact zone during wrapping and increase the adhesion with the NP, as the wrapping degree increases (Cherry 1975; Cooper et al. 2007; McCloskey et al. 1984; Serpelloni et al. 2021). The hypothesis of a constant adhesion parameter, used in the existing model, does consequently not apply and $\overline{\gamma}$ needs to be modeled as a function of the wrapping degree. The nature of this function is discussed in Section 3.2.

3.2 Model of the mechanical adaptation of the membrane

Based on the previous assumptions, the NP-membrane adhesion, $\overline{\gamma}$, is considered as a function of the wrapping degree f, leading to $\overline{\gamma} := \overline{\gamma}(f)$. The nature of the function, that will be proposed in this work, is determined according to conclusions from the experimental studies reported in the literature. Hence, one can infer that the adhesion tends to increase during the wrapping process until reaching a final value, which corresponds to the stage when all the possible bonds between constituents from the NP and the membrane are formed (Yuan et al. 2010; Yi and Gao 2017; Freund 2004). It is however unclear if the constituents responsible for adhesion (specific receptors or ligands, proteins and lipids) start moving to the contact region as soon as the NP approaches the membrane, or if there is a delay, that would correspond to the information transmission to the rest of the membrane. We assume that this process contributes to an increase in adhesion and therefore we expect the adhesion to monotonically increase with respect to the wrapping degree f, starting from an initial minimum value and reaching a maximum final value. As such, $\overline{\gamma}(f)$ is modeled using a three-parameter sigmoidal function of f. Indeed, sigmoids have already been used in biology for the modeling of measures of nerve activity in terms of the arterial pressure (Head et al. 1987; Dorward et al. 1985; Ricketts et al. 1999). They are also commonly used in other fields of mechanics to model the diffusion phenomenon (Obeid et al. 2018), which may be similar to the behavior of the constituents of the membrane along its circumference. The variation of adhesion reads

$$\overline{\gamma}(f) = \frac{\overline{\gamma}_0(\overline{\gamma}_A - 1)}{1 + \exp\left[-2\overline{\gamma}_S(f - f_{\text{inf}})\right]} + \overline{\gamma}_0 \tag{4}$$

where f_{inf} is the inflection point, defined in terms of the delay $\overline{\gamma}_D$ as $f_{\text{inf}} = 0.5 + \overline{\gamma}_D$, while $\bar{\gamma}_A$ represents the amplitude of the transition and $\bar{\gamma}_S$ is the curvature parameter, which is independent of the aforementioned parameters and is used to control the slope of $\overline{\gamma}$ at the inflection point. In terms of receptor movement, $\overline{\gamma}_D$ is the delay in wrapping degree after which the receptors start moving, $\bar{\gamma}_A$ is the ratio between the final and initial quantity of receptors in the interaction region and $\bar{\gamma}_S$ is the displacement velocity of the receptors, in terms of wrapping degree. The initial value of adhesion, *i.e.* $\overline{\gamma}(f \to 0)$, is denoted by $\overline{\gamma}_0$. These parameters are detailed in Table 1 and their contributions to $\overline{\gamma}(f)$ are schematically illustrated in Figure 5.

Table 1 Parameters of the sigmoid functions.

Parameter	Definition	Range
$\overline{\gamma}_A$	Ratio between $\overline{\gamma}(f=1)$ and $\overline{\gamma}_0$	$[1, 6]$
$\overline{\gamma}_D$	Delay of the transition, compared to $f = 0.5$	$[-0.2, 0.2]$
$\overline{\gamma}_S$	Curvature parameter	$[10, 50]$

The lower bound of the domain of definition of $\overline{\gamma}_A$ is set to 1 in order to have an increasing function, while the upper bound has been set as being approximately equal to the amplitude of the domain of definition of $\overline{\gamma}_0$, which was defined based on previous works (Iaquinta et al. 2022; Yi, Shi, et al. 2011; S. Zhang et al. 2015) as the interval $[1, 8]$. It is worth noting that the particular configuration where $\overline{\gamma}_A = 1$ corresponds to a passive membrane, in which case the parameters $\overline{\gamma}_D$ and $\overline{\gamma}_S$ have no influence since the first term of the right-hand side of Equation (4) vanishes, yielding $\overline{\gamma}(f) = \overline{\gamma}_0$. The domain of definition of $\overline{\gamma}_D$ is determined using mathematical constraints. Indeed, as the mid value of the transition from $\overline{\gamma}_0$ to $\overline{\gamma}(f \to 1)$ is reached at $f_{\text{inf}} = 0.5 + \overline{\gamma}_D$, $\overline{\gamma}_D$ should vary in $[-0.5, 0.5]$. To avoid numerical singularities and a too-early or late transition, we chose to set a smaller interval, *i.e.* $\overline{\gamma}_D \in [-0.2, 0.2]$. Finally, the domain of $\overline{\gamma}_S$ was set to represent a reasonable range of values of curvatures, while ensuring that the boundary conditions $\overline{\gamma}(0) = \overline{\gamma}_0$ and $\overline{\gamma}(1) = \overline{\gamma}_0\overline{\gamma}_A$ are respected. Note that the curvature parameter $\overline{\gamma}_S$ is used to evaluate the slope of $\overline{\gamma}(f)$ at the inflection point f_{inf} that is a function of $\overline{\gamma}_S$, $\overline{\gamma}_0$, and $\overline{\gamma}_A$.

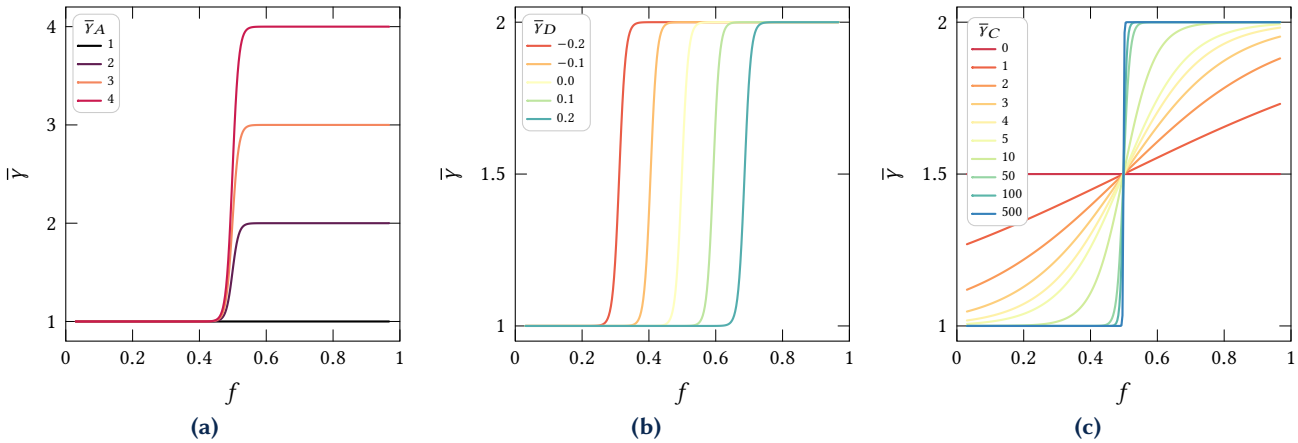

Figure 5 Effect of the parameters of an increasing sigmoid function: evolution of $\overline{\gamma}(f)$ for (a) $\overline{\gamma}_A \in \{1, 2, 3, 4\}$, (b) $\overline{\gamma}_D \in \{-0.2, -0.1, 0, 0.1, 0.2\}$ and (c) $\overline{\gamma}_S \in [0, 500]$. We set $(\overline{\gamma}_A, \overline{\gamma}_D, \overline{\gamma}_S) = (2, 0, 50)$ and $(\overline{\gamma}_0, \overline{\sigma}) = (1, 2)$ for all cases, except when stated otherwise in the graphs. Note that for the particular case, where $\overline{\gamma}_S = 0$, $\overline{\gamma}$ is independent of f and equals $\overline{\gamma}_0(\overline{\gamma}_A + 1)/2 = 1.5$, wherein none of the boundary conditions are satisfied.

4 Influence of the mechano-adaptation of the membrane on the predictions of the model

4.1 Method

4.1.1 Definition of the QoI

Once the function describing the evolution of $\overline{\gamma}$ is set, it is necessary to determine whether, and to which extent, the modeling of $\overline{\gamma}$ as a function instead of a constant, influences the results of the model. For this purpose, a global sensitivity analysis is conducted by calculating the Sobol indices. In this study, our Quantity of Interest (QoI) is ψ_3, the proportion of cells that reach the full wrapping phase. The latter is computed following several steps. (1) for each tuple $(\overline{\gamma}_0, \overline{\sigma})$, taken within the domain of definition of the variables, the variation $\overline{\Delta E}$ in terms of f is computed to identify the equilibrium position of the NP and thus (2) the equilibrium phase. The latter is used to (3) build the phase diagram, in which each region corresponds to an equilibrium phase $i \in \{1, 2, 3\}$. Finally, the phase proportions ψ_i, $i \in \{1, 2, 3\}$ are computed as the ratio of tuples $(\overline{\gamma}_0, \overline{\sigma})$ that yield the phase i over the total number of tuples. This number of tuples was set to

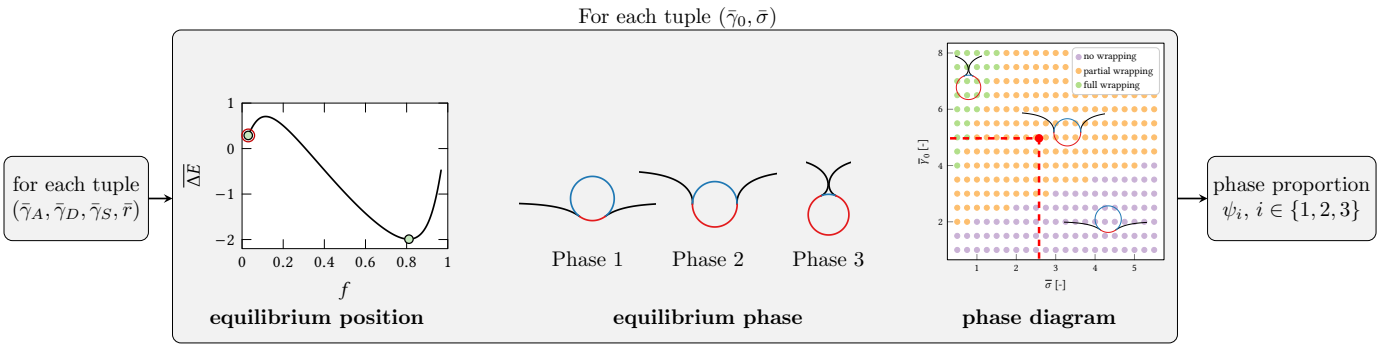

Figure 6 Description of the flux of calculation for obtaining the phase proportions $\psi_i (i \in \{1, 2, 3\})$ given the input parameters $(\overline{\gamma}_A, \overline{\gamma}_D, \overline{\gamma}_S, \overline{r})$.

280 after a convergence study on ψ_i, $i \in \{1, 2, 3\}$. An example of phase diagram is provided in Figure 7(a). Note that this phase diagram was built with more than 280 points for the purpose of the illustration. For each tuple of $(\overline{\gamma}_A, \overline{\gamma}_D, \overline{\gamma}_S, \overline{r})$, a phase diagram is built, from which ψ_3 is extracted. The flux of calculation is illustrated in Figure 6. Note that all the phase diagrams are built using a regular sampling, with the same amount of points and the same domains of definition for $\overline{\gamma}_0$ and $\overline{\sigma}$.

An illustration of the evolution of the phase proportions in the case of a mechano-adaptive membrane is provided in Figure 7(b).

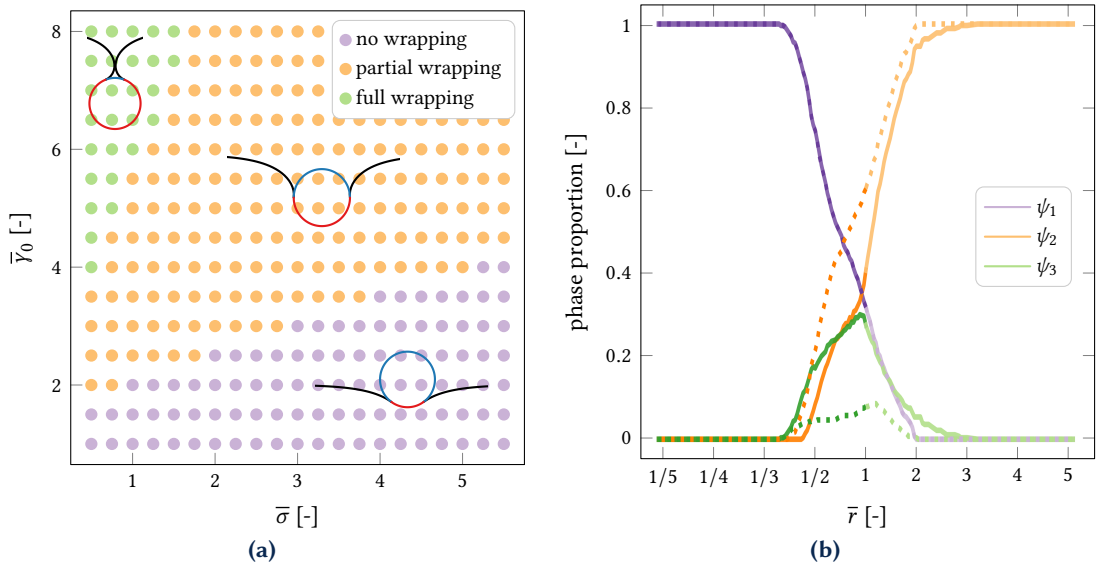

Figure 7 Wrapping phases.(a) Example of phase diagram, obtained with $(\overline{\gamma}_A, \overline{\gamma}_D, \overline{\gamma}_S, \overline{r}) = (1, 0, 10, 1)$ and displayed with 1120 points for the quality of the illustration. (b) Comparison of the evolution of the phase proportions in terms of the aspect ratio $\overline{r}$ of the NP, between a passive membrane (dotted line) and a mechano-adaptive membrane $(\overline{\gamma}_A, \overline{\gamma}_D, \overline{\gamma}_S) = (2, 0, 50)$.

4.1.2 Sampling of the input parameters

The Sobol indices are functions of the conditional variance of the QoI (see (Abramov et al. 1993) for more details). As such, the latter needs to be estimated. Such an estimation may require thousands of Monte Carlo (MC) samples in order to reach convergence (Iooss et al. 2015). In this article, we consider that the convergence of the Sobol indices is reached when the range of their 95 % confidence intervals (CI) is smaller than the threshold of 0.05. This criterion was proposed by Sarrazin et al. (2016), as it enables us to investigate the convergence of each index separately, contrary to other criteria that investigate the convergence of the sum of the sensitivity indices (Vanrolleghem et al. 2015) or that of the most important parameter (Herman et al. 2013). Considering the computational cost of our model, using it to generate that number of samples is not feasible (about 32 days to build 1000 samples, with the available computational resources). In

order to reduce the number of samples necessary to reach convergence, the dataset is constructed using the quasi Monte Carlo sampling technique, built with Sobol's sequences. In addition, a surrogate model needs to be used to evaluate the QoI faster than the model itself. For this purpose, the Kriging metamodel, also known as Gaussian process, has been constructed, using the open-source library OpenTURNS. Technical details on Kriging and its implementation for this model have been presented in (Iaquinta et al. 2022) and general information on this metamodel can be found in (Cressie 1990; Sacks et al. 1989; Stein 2012; Santner et al. 2013; Rasmussen 2004; De Lozzo et al. 2016; Marrel et al. 2008). The development of this tool will be presented in the following sections. In order to understand the effect of the parameters of the sigmoid on ψ_3, the sensitivity analysis will first be conducted on circular NPs in Section 4.2. Then, the same study will be conducted on elliptic NPs in Section 4.3 to observe the effect of these parameters, when combined with $\overline{r}$.

4.2 Uptake of circular NPs

In this case, the model has three input parameters: $\overline{\gamma}_A$, $\overline{\gamma}_D$, and $\overline{\gamma}_S$. A dataset, containing $2^{10} = 1024$ input samples of the random uniform variables $\overline{\Gamma}_A$, $\overline{\Gamma}_D$, and $\overline{\Gamma}_S$, was used to build the dataset containing the values of Ψ_3, necessary for the construction of the metamodel. Note that uniform distributions have been used to model these variables based on the maximum entropy principle (Jaynes 1957) since the only available information is the extreme values of each parameter. An estimation of the probability density function (PDF) of Ψ_3, based on this dataset, is represented in Figure 8(a). In order to determine the minimal amount of data that is necessary for testing the predictions of the metamodels, the representativeness of the dataset is investigated by computing the normalized absolute gradient of the mean and the standard deviation of Ψ_3. The latter, for a function y depending on a variable x, is defined as $|y(x+1) - y(x)|/|y(x)|$. A subdataset is considered to be representative of the behavior of the dataset when both of these first and second-order statistics are smaller than the threshold criterion, defined as 10^{-2}. According to Figures 8(b) and 8(c), the test dataset should contain at least 144 samples. The remaining dataset will therefore be used to construct the metamodels.

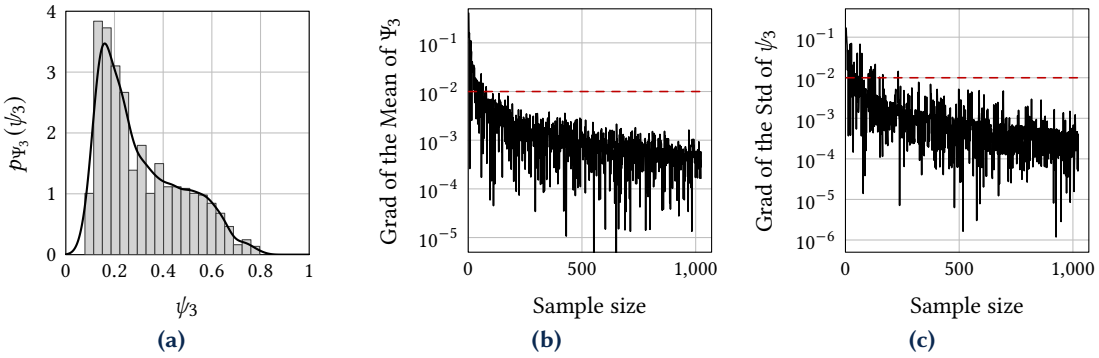

Figure 8 Observations on the Ψ_3 dataset in the case of circular NPs. (a) Estimation of the PDF of Ψ_3 based on the dataset. (b) Absolute gradient of the mean of Ψ_3, in terms of the number of samples. (c) Absolute gradient of the standard deviation of Ψ_3, in terms of the number of samples.

The Kriging metamodel has been built using a constant trend function along with a squared exponential (Gaussian) correlation function. The predictions obtained with the metamodel are compared to the values contained in the test dataset in Figure 9(a). To quantify the accuracy of the metamodel, the predictability factor Q_2 is computed. The latter is defined as

$$Q_2 = 1 - \frac{\sum_{i=1}^{N}(Y_i - \hat{Y}_i)^2}{N\mathrm{Var}(\hat{Y})} \tag{5}$$

where Y_i and $\hat{Y}_i$ are the i-th true value in the test dataset and the corresponding prediction of the QoI, respectively. The metamodel yielded $Q_2 = 0.99$. Figure 9(b) compares the estimation of the PDF of the predictions generated via Kriging to that of the model, using the responses of the metamodel to 10^5 MC-based input samples. In conclusion, Kriging can be used to

perform the sensitivity analysis, which will be presented in the following, as it provides accurate approximations of the model.

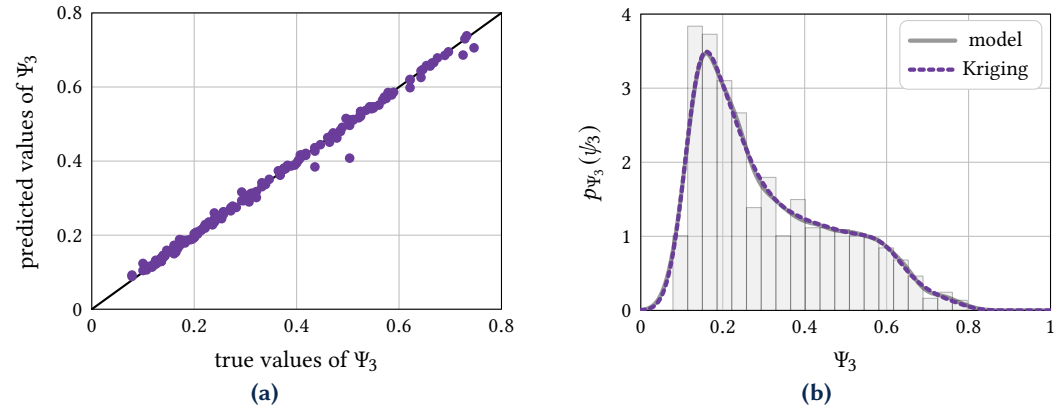

Figure 9 Kriging predictions. (a) Predicted vs true values obtained with Kriging. (b) Comparison of the PDFs estimated from the predictions of this metamodel to that obtained from the model.

The Sobol sensitivity indices have been estimated with the Saltelli (Saltelli 2002), Mauntz-Kucherenko (Sobol' et al. 2007), Martinez (Baudin et al. 2016) and Jansen (Jansen 1999) algorithms, implemented in OpenTURNS. Once the convergence is reached, the Sobol indices become independent of the algorithm. The range of the 95 % CIs, in terms of the number of estimations, are depicted in Figure 10.

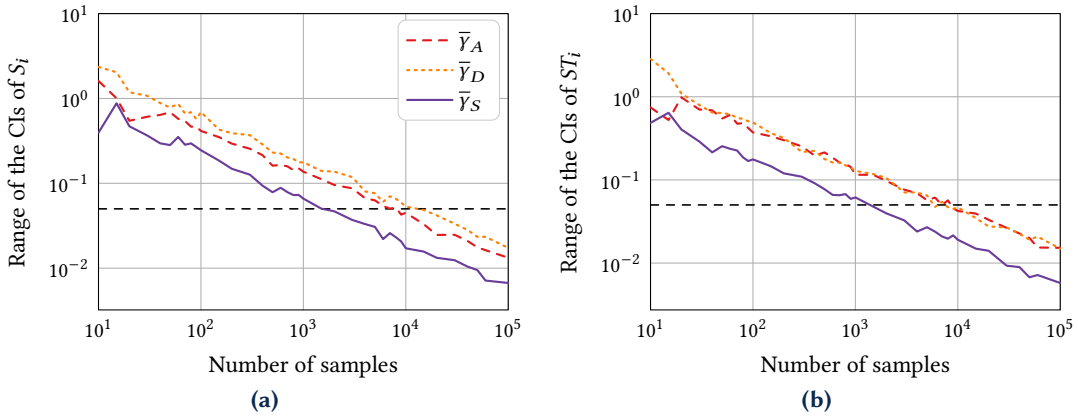

Figure 10 Convergence of the Sobol indices. (a) First order Sobol indices. (b) Total Sobol indices. Ranges of the 95 % confidence intervals in terms of the number of estimations of the metamodel, computed using the Mauntz-Kucherenko algorithm. The black dashed lines correspond to a threshold of 0.05.

The converged Sobol indices are summarized in Table 2. These values reveal that the most important variable is the delay of the transition, $\overline{\gamma}_D$, with a total index of 0.64. Its first order index is 0.5, implying that the Sobol index relative to the interactions of $\overline{\gamma}_D$ with $\overline{\gamma}_A$ and $\overline{\gamma}_S$ are $0.64 - 0.50 = 0.14$. Furthermore, since the interactions of $\overline{\gamma}_S$ are negligible (the first and total indices are close), $\overline{\gamma}_D$ interacts mostly with $\overline{\gamma}_A$, which is the amplitude of the transition. The latter is the second most influential parameter on the variance of Ψ_3 ($ST_{\overline{\gamma}_A} = 0.43$) and the interactions of $\overline{\gamma}_D$ with $\overline{\gamma}_A$ and $\overline{\gamma}_S$ contribute by $100 \times 0.14/0.43 = 33\%$ to the effect of $\overline{\gamma}_A$ on Ψ_3. These results lead to the conclusion that $\overline{\gamma}_D$ is the most important parameter, followed by $\overline{\gamma}_A$, which contributes to the output almost twice as less as $\overline{\gamma}_D$. The interactions between these two variables also contribute to the variance of the output. Last, $ST_{\overline{\gamma}_S} = 0.10$, which, even if it is small, is not negligible compared to the order of magnitude of the contribution of the other parameters.

4.3 Uptake of elliptic NPs

In this section, the study conducted previously is applied to elliptic NPs, whose aspect ratio $\overline{r}$ is defined as the ratio between the semi-minor and semi-major axes. Hence, $\overline{r}$ is smaller (resp.

Table 2 First and total Sobol indices, calculated using 10^5 estimations of the metamodel.

Index	Parameter	Estimation
S_i	$\overline{\gamma}_A$	0.28
	$\overline{\gamma}_D$	0.50
	$\overline{\gamma}_S$	0.07
ST_i	$\overline{\gamma}_A$	0.43
	$\overline{\gamma}_D$	0.64
	$\overline{\gamma}_S$	0.10

larger) than 1 for vertical (resp. horizontal) NPs, and the particular case where $\overline{r} = 1$ stands for circular NPs. In this study, we investigate NPs whose aspect ratios range from 1/6 to 6. The random variable $\overline{R}$ is added to the set of input parameters. As such, the problem contains four input parameters and the QoI is still Ψ_3. The distribution of $\overline{R}$ is built so that half of the dataset contains horizontal NPs ($1 < \overline{R} < 6$), and the remaining half of the values of $\overline{R}$ are the inverse of the aspect ratios of the horizontal ellipses. Hence, the distribution of $\overline{R}$ for $\overline{R} < 1$ should be the inverse of the uniform distribution used to maximize the entropy for the distribution of the horizontal NPs, leading to the PDF

$$f_{\overline{R}}(x) = \begin{cases} \dfrac{1}{2}\dfrac{1}{6-1}\dfrac{1}{x^2} = \dfrac{1}{10}\dfrac{1}{x^2} & \text{for } x \in [1/6, 1[\\ \dfrac{1}{2}\dfrac{1}{6-1} = \dfrac{1}{10} & \text{for } x \in]1, 6] \\ 0 & \text{otherwise.} \end{cases} \tag{6}$$

The distribution of Ψ_3 is depicted in Figure 11(a). According to the absolute normalized gradient of the mean and standard deviation of Ψ_3, represented respectively in Figures 11(b) and 11(c), the test dataset requires to contain at least 365 samples. One can note that more samples are necessary compared to the previous case, which is due to the addition of the input parameter $\overline{R}$.

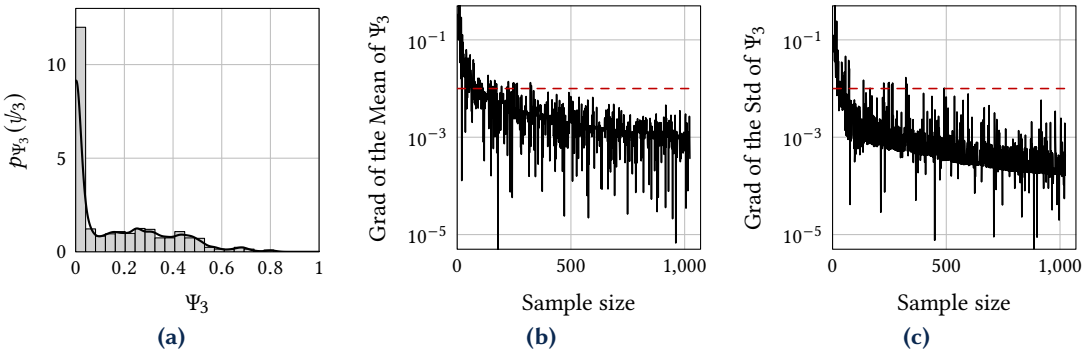

Figure 11 Observations on the psi_3 dataset in the case of elliptic NPs. (a) Estimation of the PDF of Ψ_3 based on the dataset. (b) Absolute gradient of the mean of Ψ_3, in terms of the number of samples. (c) Absolute gradient of the standard deviation of Ψ_3, in terms of the number of samples.

Here again, the Kriging metamodel is built in order to generate estimations of the model, necessary to further evaluate the Sobol indices. The Kriging metamodel was constructed with the same hyperparameters as those used in the previous case, yielding $Q_2 = 0.92$, based on the prediction presented in Figure 12(a). An estimation of the PDF of the predictions of Ψ_3 using 10^5 MC-based generated input samples is represented in Figure 12(b). According to these results, the predictions from Kriging can be used to estimate the Sobol indices, since they are able to reproduce the behavior of the model. However, it is worth noting that this metamodel yields some inaccurate predictions, that may influence the precision of the Sobol indices, computed in the following.

The convergence of the Sobol indices, in terms of the number of estimations, is depicted in Figure 13. The convergence is ensured when at least 2×10^4 estimations are used. The converged values are summarized in Table 3.

This study highlights that $\overline{r}$ is the most influential parameter, with the largest total Sobol index, $ST_{\overline{r}} = 0.72$, while the curvature parameter $\overline{\gamma}_S$ is the less influential parameter with the

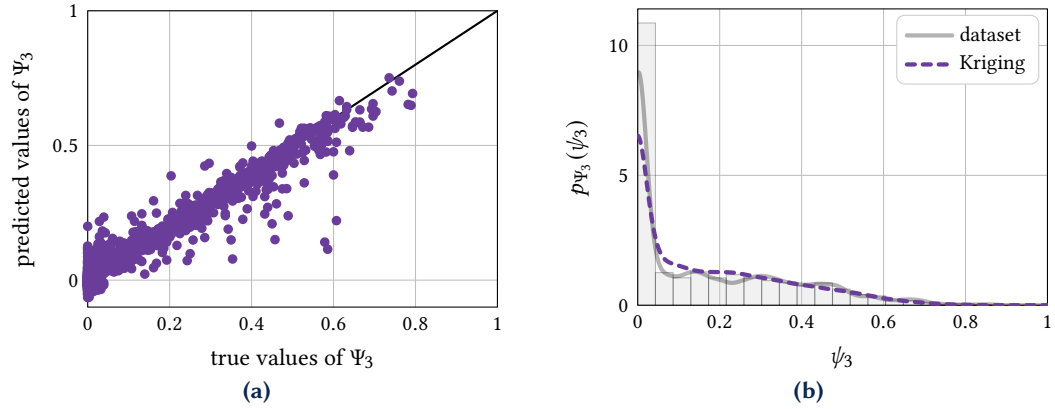

Figure 12 Kriging predictions. (a) Predicted vs true values. (b) Comparison of the PDFs estimated via this metamodel.

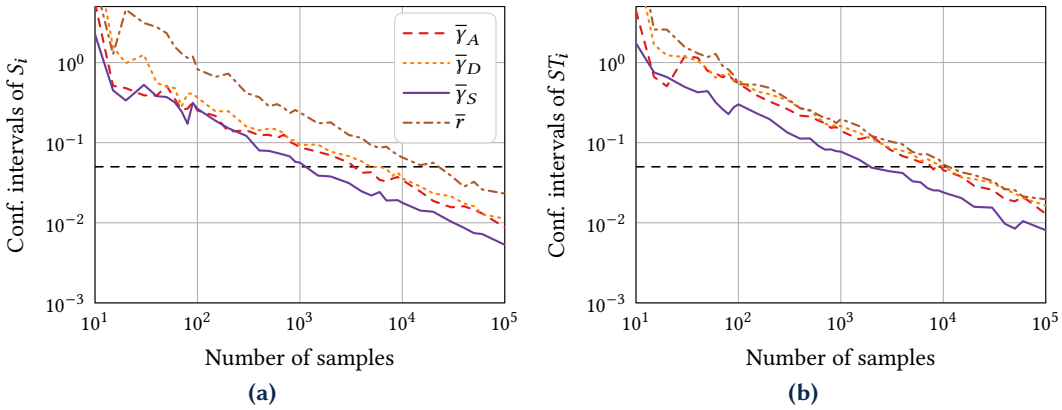

Figure 13 Convergence of the Sobol indices. (a) First order Sobol indices. (b) Total Sobol indices. Ranges of the 95 % confidence intervals in terms of the number of estimations of the metamodel, computed using the Mauntz-Kucherenko algorithm. The black dashed lines correspond to a threshold of 0.05.

lowest total Sobol index, $ST_{\overline{\gamma}_S} = 0.07$. Its first-order index is almost zero ($S_{\overline{\gamma}_S} = 0.02$), meaning that its influence on Ψ_3, is primarily due to interactions with other parameters $\overline{\gamma}_A$, $\overline{\gamma}_D$ and $\overline{r}$. A similar observation is made for the amplitude of the transition, $\overline{\gamma}_A$, whose first-order Sobol index is small ($S_{\overline{\gamma}_A} = 0.09$). The parameter with the largest total Sobol index, after $\overline{r}$, is the transition delay $\overline{\gamma}_D$, with $ST_{\overline{\gamma}_D} = 0.33$. It is thus the second most influential parameter. Still, its first-order index ($S_{\overline{\gamma}_D} = 0.11$) is small compared to the total index, meaning that the effect of $\overline{\gamma}_D$ is mainly due to its interactions with the remaining parameters. The curvature parameter and the amplitude of the transition, $\overline{\gamma}_S$ and $\overline{\gamma}_A$ being of small importance, one can infer that the influence of $\overline{\gamma}_D$ on Ψ_3 is mostly due to interactions with the aspect ratio $\overline{r}$ of the NP. One can also note that the ranking of importance between the parameters $\overline{\gamma}_A$, $\overline{\gamma}_D$, and $\overline{\gamma}_S$ is the same as the one obtained for circular NPs ($\overline{r} = 1$), as illustrated in Figure 14.

5 Discussion

The Kriging metamodel used to generate estimations of the model in the case of circular NPs yielded accurate predictions ($Q_2 = 0.99$). The same model, applied to elliptic NPs, could not be approximated with the same accuracy via Kriging ($Q_2 = 0.92$), showing that $\overline{r}$ induced nonlinearities that could not be handled by this metamodel. Alternative surrogate modeling approaches could have been tested, *e.g.* Polynomial Chaos Expansion (PCE), PCE-Kriging, and artificial neural networks, that may provide different and potentially better predictions. Hence, it would be of great interest to investigate these methods to improve the accuracy of the estimations used to compute the Sobol indices. Furthermore, PCE could be used to analytically calculate the Sobol indices based on the expansion coefficients (Sudret 2008). In addition, the output of Kriging could be post-processed to clip the predictions within the domain of definition of the QoI. As such, each estimation smaller than the lower bound would be replaced by the bound that has not

Table 3 First and total Sobol indices, calculated using 10^5 estimations of the metamodel.

Index	Parameter	Estimation
S_i	$\overline{\gamma}_A$	0.07
	$\overline{\gamma}_D$	0.18
	$\overline{\gamma}_S$	0.02
	$\overline{r}$	0.47
ST_i	$\overline{\gamma}_A$	0.25
	$\overline{\gamma}_D$	0.34
	$\overline{\gamma}_S$	0.09
	$\overline{r}$	0.79

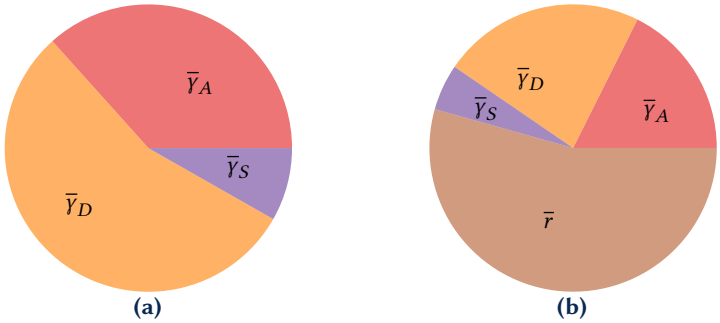

Figure 14 Distribution of the total Sobol indices obtained in (a) the investigation of the influence of $\overline{\gamma}_A$, $\overline{\gamma}_D$ and $\overline{\gamma}_S$ on the uptake of a circular NP and in (b) the comparison of the influence of $\overline{\gamma}_A$, $\overline{\gamma}_D$ and $\overline{\gamma}_S$ to that of the aspect ratio $\overline{r}$ of an elliptic NP.

been respected, which would compensate the under-estimations. Furthermore, little is known about the input parameters, especially those of the sigmoid used to describe the variation of the adhesion between the NP and the cell membrane during the wrapping process. Hence, the domain of definition of these parameters was set following inferences based on observations reported in the literature, along with mathematical considerations. Given that the domain of definition of a variable affects the sensitivity analyses (Cousin et al. 2019), conducting a study in which the bounds vary could consequently allow us to quantify the dependence of the results of the sensitivity analyses on the domains of definition of the parameters. A similar remark can be made concerning the influence of the statistical distribution of these parameters on the sensitivity analysis, as it is also likely to alter the results. Furthermore, the model investigated in this article focuses on wrapping, which only one step of endocytosis. The prior and additional steps (eg clearance and exocytosis) also need to be considered to consider the likeliness of cellular internalization of a nanoparticle. The major contribution of the NP's aspect ratio matches experimental observations from the literature. For instance, Champion, Katare, et al. (2007); Champion and Mitragotri (2006) highlighted that the entry of a NP within macrophages, whose adhesion has not been controlled, is dictated by the NP's aspect ratio.

6 Conclusion

In this article, we have presented an enrichment of the existing model of the cellular uptake of rigid elliptic NPs, at the scale of the NP, by accounting for the mechanical adaptation of the membrane. This phenomenon was described using a sigmoidal variation of the NP-membrane adhesion, in terms of the wrapping degree of the membrane. To quantify the influence of the parameters that have been introduced, sensitivity analyses have been conducted, in the case of the uptake of circular and elliptic NPs. They showed that the aspect ratio of the NP influences Ψ_3 as much as the parameters related to the variation of $\overline{\gamma}$, among which the delay $\overline{\gamma}_D$ of the transition is the most important, followed by its amplitude $\overline{\gamma}_A$, while the curvature parameter $\overline{\gamma}_S$ can be considered as non-influential. The mechanical adaptation of the membrane plays therefore an important role in the predictions of the model. The values of $\overline{\gamma}_D$ and $\overline{\gamma}_A$ should consequently be precisely determined, based on experimental investigations, to obtain accurate predictions of cellular internalization of NPs. In addition, the results presented in this article revealed that the

aspect ratio of the NP is the most important parameter in the case of an adaptive membrane, which was also the case when the adaptation of the membrane was not considered (Iaquinta et al. 2022). Consequently, efforts should first be made on the precision and repeatability of the manufacturing of NPs. Second, additional investigations should be performed to accurately measure the transition delay and the amplitude of the variation of the adhesion between the cell membrane and the NP.

7 Bibliography

Abramov, V., A. Kartashev, and A. Roshal' (1993). Sensitivity analysis for non-linear mathematical models. *USSR Computational Mathematics and Mathematical Physics* 26(2):93–97. [DOI].

Baudin, M., A. Dutfoy, B. Iooss, and A.-L. Popelin (2016). OpenTURNS: An Industrial Software for Uncertainty Quantification in Simulation. *Handbook of Uncertainty Quantification*. Ed. by R. Ghanem, D. Higdon, and H. Owhadi. Springer, pp 1–38. [DOI].

Briolay, T., T. Petithomme, M. Fouet, N. Nguyen-Pham, C. Blanquart, and N. Boisgerault (2021). Delivery of cancer therapies by synthetic and bio-inspired nanovectors. *Molecular Cancer* 20(1):1–24. [DOI], [OA].

Canton, I. and G. Battaglia (2012). Endocytosis at the nanoscale. *ChemInform* 43(27):2718–2739. [DOI].

Champion, J. A., Y. K. Katare, and S. Mitragotri (2007). Making polymeric micro-and nanoparticles of complex shapes. *Proceedings of the National Academy of Sciences* 104(29):11901–11904. [DOI], [OA].

Champion, J. A. and S. Mitragotri (2006). Role of target geometry in phagocytosis. *Proceedings of the National Academy of Sciences* 103(13):4930–4934. [DOI], [OA].

Cherry, R. J. (1975). Protein mobility in membranes. *FEBS Letters* 55(1–2):1–7. [DOI], [OA].

Chu, E. (2017). Cancer Chemotherapy. *Basic & Clinical Pharmacolog*. Ed. by B. G. Katzung. 14th ed. Chapter 54. McGraw-Hill Education, pp 1–39. ISBN: 9781259641152.

Chu, Y.-S., S. Dufour, J. P. Thiery, E. Perez, and F. Pincet (2005). Johnson-Kendall-Roberts theory applied to living cells. *Physical Review Letters* 94(2):028102. [DOI], [ARXIV].

Cooper, G. M. and R. E. Hausman (2007). *The cell: a molecular approach*. 6th ed. ASM press. ISBN: 9780878939640.

Cousin, A., A. Janon, V. Maume-Deschamps, and I. Niang (2019). On the consistency of Sobol indices with respect to stochastic ordering of model parameters. *ESAIM: Probability and Statistics* 23:387–408. [DOI], [OA].

Cressie, N. (1990). The origins of kriging. *Mathematical Geology* 22(3):239–252. [DOI].

De Lozzo, M. and A. Marrel (2016). Estimation of the derivative-based global sensitivity measures using a Gaussian process metamodel. *SIAM/ASA Journal on Uncertainty Quantification* 4(1):708–738. [DOI], [HAL].

Decuzzi, P. and M. Ferrari (2008). The receptor-mediated endocytosis of nonspherical particles. *Biophysical Journal* 94(10):3790–3797. [DOI], [OA].

Deserno, M. and T. Bickel (2003). Wrapping of a spherical colloid by a fluid membrane. *Europhysics Letters (EPL)* 62(5):767–774. [DOI], [ARXIV].

Deserno, M. (2004). Elastic deformation of a fluid membrane upon colloid binding. *Physical Review E* 69(3):031903. [DOI], [OA].

Dorward, P. K., W. Riedel, S. L. Burke, J. Gipps, and P. I. Korner (1985). The renal sympathetic baroreflex in the rabbit. Arterial and cardiac baroreceptor influences, resetting, and effect of anesthesia. *Circulation Research* 57(4):618–633. [DOI], [OA].

Evans, E. and D. Needham (1987). Physical properties of surfactant bilayer membranes: thermal transitions, elasticity, rigidity, cohesion and colloidal interactions. *The Journal of Physical Chemistry* 91(16):4219–4228. [DOI].

Ferguson, J. P., S. D. Huber, N. M. Willy, E. Aygün, S. Goker, T. Atabey, and C. Kural (2017). Mechanoregulation of clathrin-mediated endocytosis. *Journal of Cell Science* 130(21):3631–3636. [DOI], [OA].

Ferlay, J., M. Colombet, I. Soerjomataram, D. M. Parkin, M. Piñeros, A. Znaor, and F. Bray (2021). Cancer statistics for the year 2020: An overview. *International Journal of Cancer*

149(4):778–789. [DOI], [OA].

Freund, L. (2004). The role of binder mobility in spontaneous adhesive contact and implications for cell adhesion. *Journal of the Mechanics and Physics of Solids* 52(11):2455–2472. [DOI].

Gerber, D. E. (2008). Targeted therapies: a new generation of cancer treatments. *American family physician* 77(3):311–319.

Haley, B. and E. Frenkel (2008). Nanoparticles for drug delivery in cancer treatment. *Urologic Oncology: Seminars and Original Investigations* 26(1):57–64. [DOI], [OA].

Hall, A. (2009). The cytoskeleton and cancer. *Cancer and Metastasis Reviews* 28(1–2):5–14. [DOI].

Head, G. A. and R. McCarty (1987). Vagal and sympathetic components of the heart rate range and gain of the baroreceptor-heart rate reflex in conscious rats. *Journal of the Autonomic Nervous System* 21(2–3):203–213. [DOI].

Helfrich, W. (1973). Elastic properties of lipid bilayers: theory and possible experiments. *Zeitschrift für Naturforschung C* 28(11–12):693–703. [DOI], [OA].

Hellerstedt, B. A. and K. J. Pienta (2002). The current state of hormonal therapy for prostate cancer. *CA: A Cancer Journal for Clinicians* 52(3):154–179. [DOI], [OA].

Herman, J. D., J. B. Kollat, P. M. Reed, and T. Wagener (2013). Method of Morris effectively reduces the computational demands of global sensitivity analysis for distributed watershed models. *Hydrology and Earth System Sciences* 17(7):2893–2903. [DOI], [OA].

Iaquinta, S., S. Khazaie, É. Ishow, C. Blanquart, S. Fréour, and F. Jacquemin (2022). Influence of the mechanical and geometrical parameters on the cellular uptake of nanoparticles: a stochastic approach. *International Journal for Numerical Methods in Biomedical Engineering* 38(6):e3598. [DOI], [HAL].

Iooss, B. and P. Lemaître (2015). A review on global sensitivity analysis methods. *Uncertainty Management in Simulation-Optimization of Complex Systems*. Vol. 59. Operations Research/Computer Science Interfaces Series. Springer, pp 101–122. [DOI], [ARXIV].

Jansen, M. J. (1999). Analysis of variance designs for model output. *Computer Physics Communications* 117(1–2):35–43. [DOI].

Jaynes, E. T. (1957). Information theory and statistical mechanics. *Physical Review* 106(4):620–630. [DOI].

Kanyo, N., K. D. Kovacs, A. Saftics, I. Szekacs, B. Peter, A. R. Santa-Maria, F. R. Walter, A. Dér, M. A. Deli, and R. Horvath (2020). Glycocalyx regulates the strength and kinetics of cancer cell adhesion revealed by biophysical models based on high resolution label-free optical data. *Scientific Reports* 10(1):1–20. [DOI], [OA].

Kosmalska, A. J., L. Casares, A. Elosegui-Artola, J. J. Thottacherry, R. Moreno-Vicente, V. González-Tarragó, M. Á. del Pozo, S. Mayor, M. Arroyo, D. Navajas, X. Trepat, N. C. Gauthier, and P. Roca-Cusachs (2015). Physical principles of membrane remodelling during cell mechanoadaptation. *Nature Communications* 6(1):1–11. [DOI], [OA].

Kuo, J. C.-H., J. G. Gandhi, R. N. Zia, and M. J. Paszek (2018). Physical biology of the cancer cell glycocalyx. *Nature Physics* 14(7):658–669. [DOI], [OA].

Lekka, M., K. Pogoda, J. Gostek, O. Klymenko, S. Prauzner-Bechcicki, J. Wiltowska-Zuber, J. Jaczewska, J. Lekki, and Z. Stachura (2012). Cancer cell recognition: mechanical phenotype. *Micron* 43(12):1259–1266. [DOI].

Lin, H.-H., H.-K. Lin, I.-H. Lin, Y.-W. Chiou, H.-W. Chen, C.-Y. Liu, H. I.-C. Harn, W.-T. Chiu, Y.-K. Wang, M.-R. Shen, and M.-J. Tang (2015). Mechanical phenotype of cancer cells: cell softening and loss of stiffness sensing. *Oncotarget* 6(25):20946–20958. [DOI], [OA].

Marrel, A., B. Iooss, F. Van Dorpe, and E. Volkova (2008). An efficient methodology for modeling complex computer codes with Gaussian processes. *Computational Statistics & Data Analysis* 52(10):4731–4744. [DOI], [ARXIV].

McCloskey, M. and M.-M. Poo (1984). Protein diffusion in cell membranes: some biological implications. *International Review of Cytology* 87:19–81. [DOI].

Murphy, C. C., L. K. Bartholomew, M. Y. Carpentier, S. M. Bluethmann, and S. W. Vernon (2012). Adherence to adjuvant hormonal therapy among breast cancer survivors in clinical practice: a systematic review. *Breast Cancer Research and Treatment* 134(2):459–478. [DOI], [OA].

Nygren, P. (2001). What is cancer chemotherapy? *Acta Oncologica* 40(2–3):166–174. [DOI], [OA].

Obeid, H., A. Clément, S. Fréour, F. Jacquemin, and P. Casari (2018). On the identification of the

coefficient of moisture expansion of polyamide-6: Accounting differential swelling strains and plasticization. *Mechanics of Materials* 118:1–10. [DOI].

Rädler, J. O., T. J. Feder, H. H. Strey, and E. Sackmann (1995). Fluctuation analysis of tension-controlled undulation forces between giant vesicles and solid substrates. *Physical Review E* 51(5):4526–4536. [DOI].

Rasmussen, C. E. (2004). Gaussian processes in machine learning. *Lecture Notes in Computer Science*. Springer Berlin Heidelberg, pp 63–71. [DOI], [OA].

Ricketts, J. H. and G. A. Head (1999). A five-parameter logistic equation for investigating asymmetry of curvature in baroreflex studies. *American Journal of Physiology-Regulatory, Integrative and Comparative Physiology* 277(2):R441–R454. [DOI].

Rigato, A. F. (2015). Characterization of cell mechanics with atomic force microscopy: Mechanical mapping and high-speed microrheology. PhD thesis. Aix-Marseille. [OA].

Sacks, J., W. J. Welch, T. J. Mitchell, and H. P. Wynn (1989). Design and analysis of computer experiments. *Statistical Science* 4(4):409–423. [DOI], [OA].

Saltelli, A. (2002). Making best use of model evaluations to compute sensitivity indices. *Computer Physics Communications* 145(2):280–297. [DOI], [HAL].

Santner, T. J., B. J. Williams, and W. I. Notz (2013). *The design and analysis of computer experiments*. Springer, pp 1–13. [DOI].

Sarrazin, F., F. Pianosi, and T. Wagener (2016). Global Sensitivity Analysis of environmental models: Convergence and validation. *Environmental Modelling & Software* 79:135–152. [DOI], [OA].

Schmid, S. L., A. Sorkin, and M. Zerial (2014). Endocytosis: past, present, and future. *Cold Spring Harbor Perspectives in Biology* 6(12):a022509–a022509. [DOI], [OA].

Schuster, M., A. Nechansky, and R. Kircheis (2006). Cancer immunotherapy. *Biotechnology Journal* 1(2):138–147. [DOI].

Seifert, U. (1991). Adhesion of vesicles in two dimensions. *Physical Review A* 43(12):6803–6814. [DOI], [OA].

Seifert, U. and R. Lipowsky (1990). Adhesion of vesicles. *Physical Review A* 42(8):4768–4771. [DOI].

Serpelloni, M., M. Arricca, C. Bonanno, and A. Salvadori (2021). Modeling cells spreading, motility, and receptors dynamics: a general framework. *Acta Mechanica Sinica* 37(6):1013–1030. [DOI], [OA].

Sinha, B., D. Köster, R. Ruez, P. Gonnord, M. Bastiani, D. Abankwa, R. V. Stan, G. Butler-Browne, B. Vedie, L. Johannes, N. Morone, R. G. Parton, G. Raposo, P. Sens, C. Lamaze, and P. Nassoy (2011). Cells respond to mechanical stress by rapid disassembly of caveolae. *Cell* 144(3):402–413. [DOI], [OA].

Sobol', I., S. Tarantola, D. Gatelli, S. Kucherenko, and W. Mauntz (2007). Estimating the approximation error when fixing unessential factors in global sensitivity analysis. *Reliability Engineering & System Safety* 92(7):957–960. [DOI], [HAL].

Staykova, M., M. Arroyo, M. Rahimi, and H. A. Stone (2013). Confined bilayers passively regulate shape and stress. *Physical Review Letters* 110(2):028101. [DOI], [OA].

Stein, M. L. (2012). *Interpolation of spatial data: some theory for kriging*. Springer. [DOI].

Sudhakar, A. (2009). History of cancer, ancient and modern treatment methods. *Journal of Cancer Science & Therapy* 01(02):i–iv. [DOI], [HAL].

Sudret, B. (2008). Global sensitivity analysis using polynomial chaos expansions. *Reliability Engineering & System Safety* 93(7):964–979. [DOI].

Suresh, S. (2007). Biomechanics and biophysics of cancer cells. *Acta Biomaterialia* 3(4):413–438. [DOI], [OA].

Vanrolleghem, P. A., G. Mannina, A. Cosenza, and M. B. Neumann (2015). Global sensitivity analysis for urban water quality modelling: Terminology, convergence and comparison of different methods. *Journal of Hydrology* 522:339–352. [DOI], [OA].

Vasir, J. K. and V. Labhasetwar (2008). Quantification of the force of nanoparticle-cell membrane interactions and its influence on intracellular trafficking of nanoparticles. *Biomaterials* 29(31):4244–4252. [DOI], [OA].

Wiegand, T., M. Fratini, F. Frey, K. Yserentant, Y. Liu, E. Weber, K. Galior, J. Ohmes, F. Braun, D.-P. Herten, S. Boulant, U. S. Schwarz, K. Salaita, E. A. Cavalcanti-Adam, and J. P. Spatz

(2020). Forces during cellular uptake of viruses and nanoparticles at the ventral side. *Nature Communications* 11(1):1–13. [DOI], [OA].

Yang, C., Y. Liu, Y. He, Y. Du, W. Wang, X. Shi, and F. Gao (2013). The use of HA oligosaccharide-loaded nanoparticles to breach the endogenous hyaluronan glycocalyx for breast cancer therapy. *Biomaterials* 34(28):6829–6838. [DOI].

Yi, X. and H. Gao (2017). Kinetics of receptor-mediated endocytosis of elastic nanoparticles. *Nanoscale* 9(1):454–463. [DOI].

Yi, X., X. Shi, and H. Gao (2011). Cellular uptake of elastic nanoparticles. *Physical Review Letters* 107(9):098101. [DOI], [OA].

Yuan, H., J. Li, G. Bao, and S. Zhang (2010). Variable nanoparticle-cell adhesion strength regulates cellular uptake. *Physical Review Letters* 105(13):138101. [DOI], [OA].

Zhang, R., X. Qin, F. Kong, P. Chen, and G. Pan (2019). Improving cellular uptake of therapeutic entities through interaction with components of cell membrane. *Drug Delivery* 26(1):328–342. [DOI], [OA].

Zhang, S., H. Gao, and G. Bao (2015). Physical principles of nanoparticle cellular endocytosis. *ACS Nano* 9(9):8655–8671. [DOI], [OA].

Zhao, W., Y. Tian, M. Cai, F. Wang, J. Wu, J. Gao, S. Liu, J. Jiang, S. Jiang, and H. Wang (2014). Studying the nucleated mammalian cell membrane by single molecule approaches. *PLoS ONE* 9(5):e91595. [DOI], [OA].

Authors' contributions Author 1 carried out most of the study, performed numerical simulations, and drafted the manuscript. Author 2 helped with implementation and numerical issues. All authors developed the methodology, conceived of the study, and participated in its design, coordination, and critical review of the manuscript. All authors read and approved the final manuscript.

Supplementary Material The Python code containing the model of the cellular uptake of rigid circular and elliptic NPs, along with the routines to obtain ψ_3 is available at the permalink 10.5281/zenodo.12519966. It also contains the data and methods used to implement and validate Kriging metamodel, as well as algorithms used to compute the Sobol indices.

Acknowledgements The authors are very thankful to Dr. Christophe Blanquart and Prof. Elena Ishow for their excellent long-term collaboration and support.

Funding i-Site NExT, Région Pays de la Loire and CNRS (French National Centre for Scientific Research) through the ENAMEL project, Grant/Award Number: ANR-16-IDEX-0007.

Competing interests The authors declare that they have no competing interests.

Journal's Note JTCAM remains neutral with regard to the content of the publication and institutional affiliations.